Pre-deposited heavily P-doped a-Si:H as Dopant Source in n^+/p Junctions for Photovoltaic Applications

Rúben Pereira
ruben.pereira@tecnico.ulisboa.pt

Instituto Superior Técnico, Lisboa, Portugal

November 2018

Resumo
The c-Si main liability, in respect to the other solar cell technologies, relies on its production cost. In this work a novel method for producing c-Si pn homojunctions, which replaces two steps at high temperatures from the conventional method, was improved for photovoltaic applications. The innovation is an heavily P-doped hydrogenated amorphous silicion (a-Si:H) thin film used as dopant source. The a-Si:H is deposited by Plasma Enhanced Chemical Vapor Deposition (PECVD) at low temperature (70 °C) on a lightly doped p-type c-Si wafer. Increasing the temperature allows the dopant contained in the amorphous silicon to diffuse to the c-Si, the so-called "drive-in". Interesting results were achieved with a study that focused on the superficial dopant concentration and the homojunction depth. Moreover, a better performance of these c-Si homojunctions was accomplished by optimization of their metal contacts.
Keywords: Solar Cell, PN junctions, PECVD, Silicon, Junction Depth

1. Introduction

Climate change is one of the primary concerns for humanity in the 21st century. The increasing concentration of greenhouse gases, in particular carbon dioxide (CO_2), due to the excessive use of fossil fuels is acting to trap the heat radiated from Earth's surface causing global warming [23]. The reduction of CO_2 emissions can be achieved by switching from fossil fuels to renewable energy sources (RES). Currently, RES supplies 14% of the total world energy demand [24]. It is expected that the share of RES will increase very significantly (by 30–80% in 2100) [25].

Solar energy is the most abundant of the RES. It is emitted at a rate of 3.8×10^{23} kW, of which, approximately 1.8×10^{14} kW is intercepted by the Earth [21]. This is several times larger than the total world energy consumption [26], making photovoltaics (PV) a powerful technology.

PV was born in 1839, when the physicist Alexandre-Edmund Becquerel observed that "electrical currents arose from certain light induced chemical reactions". But it was only in 1954 that the first silicon solar cell was developed with an efficiency $\eta = 6\%$ [4].

Since the 1950s a variety of solar cell technologies arose such as thin film solar cells, dye-sensitized cells and more lately organic cells. However, wafer-based Crystalline Silicon(c-Si) is still the most popular technology, with a total market share of >90%, due to the nearly ideal band gap (Eg = 1.12 eV) and high efficiency (25.1%) [15]. The c-Si main liability, in respect to the other technologies, relies on its production cost [2]. Even though the greater part of the c-Si solar cell cost is due to the wafer itself [17], an improvement on the c-Si pn homojunction production may reduce the manufacturing cost.

A novel method for producing c-Si pn homojunctions is used in previous published work [6]. The innovation is an heavily P-doped hydrogenated amorphous silicion (a-Si:H) thin film as dopant source. The a-Si:H is deposited by Plasma Enhanced Chemical Vapor Deposition (PECVD) at low temperature (70 ° C) on a lightly doped p-type c-Si wafer. Increasing the temperature allows the dopant contained in the amorphous silicon to diffuse to the c-Si, the so-called "drive-in". This process replaces two steps at high temperatures from the conventional method: the oxidation mask (1000-1100 ° C) and the predeposition (800-1000 ° C) which makes it energetically more efficient [8]. Solar cells have been produced with an efficiency $\eta = 3.4\%$, without optimisation of the method. [5].

The main goal of this thesis is the improvement of this novel method for the production of solar cells. A primary study entitled *P-Diffusion Analysis* focused on the "drive-in"step, where particular

emphasis was given to the superficial dopant concentration and to the homojunction depth. A secondary study designated *Metal Contacts Application* was handled, which attempted to improve the performance of the solar cells described in the previous by thickening the metal contacts.

2. Background

2.1. The Solar Cell I-V Characteristic

A solar cell is an electrical device that converts the energy of the sunlight directly into electricity by the photovoltaic effect [3]. The output current of the ideal solar cell I is equal to the difference between the photocurrent I_l and the junction's electrical current. It is expressed as follows [20]:

$$I = I_0\Big[\exp\Big(\frac{qV}{kT}\Big) - 1\Big] - I_l. \tag{1}$$

It can be noted from eq. (1) that under open circuit (I=0), the photocurrent passes through the junction. On the other hand, under short circuit (V=0) the photocurrent flows through the external circuit. The ideal solar cell I-V characteristic is graphically represented in Fig. 1, where V_{mp} is the voltage at maximum power point MPP and I_{mp} is the current at MPP.

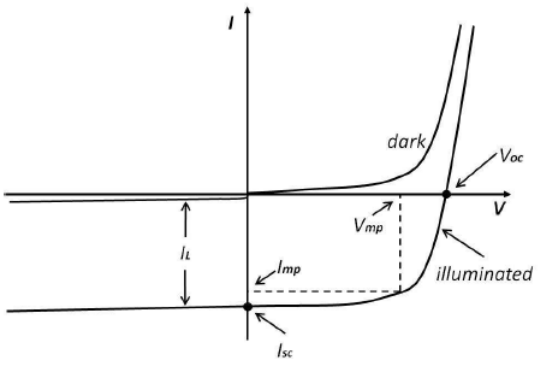

Figura 1: The ideal solar cell I-V characteristic

The I-V characteristic contains several important parameters. One is the short-circuit current I_{SC} which is equal to the photocurrent I_l. Another important parameter is the open circuit voltage V_{OC}, which represents the maximum output voltage of the solar cell at a certain illumination level. The V_{OC} can be derived from eq. 1 by setting (I=0) [20]:

$$V_{OC} = \frac{kT}{q}\ln\Big(\frac{I_l}{I_0} + 1\Big). \tag{2}$$

No power can be generated under short or open circuit. The maximum output power P_{max} produced by the solar cell, which is reached at a point on the characteristic where the IV product is maximum [19], is [20]

$$P_{max} = V_{mp}\ I_{mp}. \tag{3}$$

Given that P_{max} is less than the $I_{SC}V_{OC}$ product, the so-called fill factor FF is defined as the ratio between these two products [19],

$$FF = \frac{V_{mp}I_{mp}}{I_{SC}V_{OC}}. \tag{4}$$

Finally, the power conversion efficiency of a solar cell η, is given by [20]:

$$\eta = \frac{FFI_{SC}V_{OC}}{P_{in}}, \tag{5}$$

where P_{in} is the incident power. Therefore, in order to maximize the efficiency all three parameters in the numerator of eq. (5) should be maximized.

Although the ideal solar cell I-V characteristic can be described by 1, a real solar cell I-V characteristic is slightly different. Due not only to the resistivity of both materials used (c-Si and metal) but also to the c-Si/metal junction, a series resistance R_S must be taken into account [20]. Moreover, there are current losses in the solar cell which are represented by the shunt resistance R_{Sh} [7]. Therefore, the non-ideal I-V characteristic of the solar cell is given by [5]:

$$I = \frac{V - IR_S}{R_{Sh}} + I_0\Big[\exp\Big(\frac{qV - qIR_S}{mkT}\Big) - 1\Big] - I_l, \tag{6}$$

where m is the nonideality factor [14]. The non-ideal I-V characteristic of the solar cell (eq. (6)) may be represented by the equivalent circuit in Fig. 2.

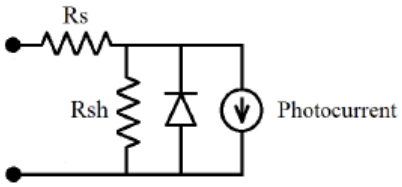

Figura 2: Equivalent circuit of a solar cell.

2.2. Novel production method

Even though solar cells are fabricated at large scale nowadays, the conventional production method can always be improved. The novel production method used during this work, replaces two steps at high temperatures from the conventional method: the oxide layer used as a diffusion mask, grown at 1000-1100 ° C and the predepostion (800-1000 ° C). The innovation is an heavily P-doped hydrogenated a-Si:H thin film as dopant source, which is deposited by PECVD at low temperature. The patterning of the diffused areas is done by photolithography

only. The method comprises the six following main steps [6, 8, 5]:

1. Preliminary lift-off photolithography for junction area delimitation.
2. The heavily P-doped a-Si:H thin film is deposited by PECVD at T = 70 °C on a lightly doped p-type c-Si wafer, using as gas precursors silane SiH_4 and phosphine PH_3.
3. Lift-off of the pre-deposited layer
4. Dehydrogenation of the a-Si:H in the diffusion furnace at T ≈ 350-550 °C.
5. The "drive-in"in the diffusion furnace at T ≈ 900-1000 °C along with the thermal oxidation of the former a-Si layer.
6. Removal of the pre-deposited layer by wet chemical etching.

This method has three main advantages: it avoids the high temperatures involved in the conventional dopant pre-deposition, the use of PECVD allows the a-Si:H deposition in a specific pattern with high precision, and it avoids the oxidation mask which also requires an high temperature process [6, 8, 5].

2.3. Diffusion

The introduction of P atoms into the lightly doped p-type c-Si wafer can be done by diffusion [10]. Diffusion is the redistribution of an initially localized substance (impurity) throughout a background medium due to random thermal motion [12]. There are three diffusion mechanisms (see Fig. 3): vacancy, interstitial and interstitialcy (which is a combination of the previous two). The interstitial mechanism occurs when the impurity atoms move along the interstitial positions of the crystal structure. Due to the atom size, the P impurities diffuse into c-Si predominantly by exchanging lattice positions with a vacancy, the vacancy mechanism. Diffusion is mathematically described by Fick's laws [16].

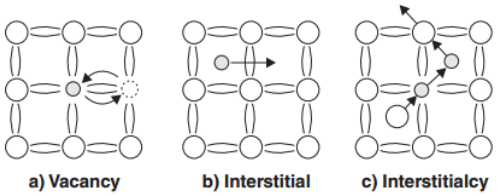

Figura 3: Vacancy, interstitial and interstitialcy mechanisms [12].

Fick's first law states that a solute will move from a region of high concentration to a region of low concentration. It relates the diffusive flux, under the assumption of steady state, to the concentration gradient by the following equation [20]:

$$J = -D\ \nabla C, \tag{7}$$

where J is the flux, D is the diffusivity and C is the concentration. Fick's second law relates the change in concentration with time to the rate at which the concentration gradient changes with distance in a given direction [20],

$$\frac{\partial C}{\partial t} = D\ \frac{\partial^2 C}{\partial x^2}. \tag{8}$$

The logarithm of the diffusivity varies proportionally to the reciprocal of the absolute temperature, T [11]. Therefore, the diffusivity can be expressed as follows [20]:

$$D = D_0\ \exp\Big(\frac{-E_A}{kT}\Big), \tag{9}$$

where D_0 is the diffusivity extrapolated to infinite temperature and E_A is the activation energy.

The dopant diffusion profile is dependent on the initial and boundary conditions. During a drive-in, where the amount of dopant is constant, the boundary conditions are [20]:

$$\int_0^\infty C(x,t)\ dx = S, \tag{10a}$$

and

$$C(\infty, t) = 0, \tag{10b}$$

where S is the total amount of dopant per unit area. Given that the initial condition is [20]

$$C(x, 0) = 0, \tag{11}$$

the solution of eq. (8) for the stated conditions is [20]

$$C(x,t) = \frac{S}{\sqrt{\pi D t}}\ \exp\Big(\frac{-x^2}{4Dt}\Big). \tag{12}$$

The surface concentration C_S is given by eq. (12), at $x = 0$ [20]:

$$C_S(t) = \frac{S}{\sqrt{\pi D t}}. \tag{13}$$

A typical concentration profile of diffused P in B-doped c-Si is shown in Fig. 4. The B-dopant concentration is represented by the so-called background concentration (C_B). The junction depth (x_j) is the depth at which concentration of acceptors is equal to the concentration of donors, it is a crucial parameter in a n+/p homojunction.

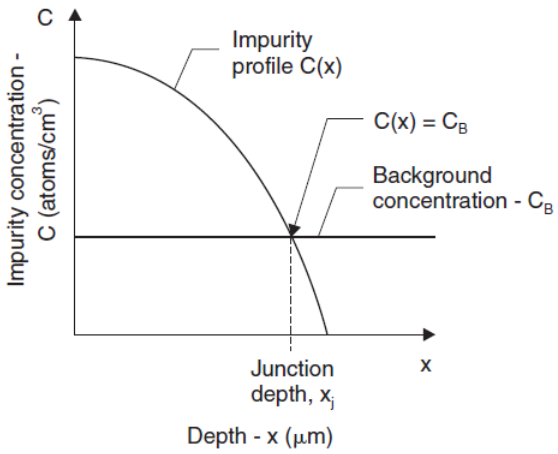

Figura 4: Impurity concentration profile, background concentration and junction depth [12].

3. Implementation

3.1. P-Diffusion Analysis

In order to determine C_s and x_j, it must be taken into consideration that upon such high P-concentrations the kink-and-tail profiles can occur due to dual diffusion mechanism involving point defects of different origins and charge states [1]. In previous work done at LMSCE, it was obtained the P-concentration profile for a diffusion at T=1000°C using the SIMS (Secondary Ion Mass Spectrometer) technique [5]. The profiles obtained evidenced high correlation with eq. 8 and the diffusivity was computed: $D = 1.3 \times 10^{-11}$ cm^2/min for 1000° C [13]. The P-concentration in the a-Si:H film, as deposited and after the dopant diffusion, was also measured with SIMS. It was determined that, for [PH3] = 1.5%, the dopant concentration 10^{21} at/cm^3 and that it remains constant throughout the a-Si:H film thickness [6] [8].

The concentration and junction depth value ranges which maximize the P-doped c-Si solar cells efficiency ($5\times10^{18} < C_s < 5\times10^{19}$ at/cm^3 and $1.2 < x_j < 2$ μm) were determined by *Steam et al* [18]. The c-Si solar cell with the highest efficiency (5.9 %) produced at the LMSCE prior to the beggining of this work has an n$^+$/p homojunction with C_s= 5×10^{19} at/cm^3 and x_j= 1.4 μm [8], both parameters in the range values mentioned previously.

In a first attempt four different n$^+$/p homojunctions (samples A,B, C and D) were fabricated multiplexing $C_s = 5 \times 10^{18}$ at/cm^3 and $C_s = 5 \times 10^{19}$ at/cm^3 with x_j= 1 μm and x_j= 2 μm, as shown in Table 1.

Sample	C_s (at/cm^3)	x_j (μm)
A	5×10^{19}	1
B	5×10^{18}	1
C	5×10^{19}	2
D	5×10^{18}	2

Tabela 1: The C_s and x_j parameters of the A, B, C and D samples.

Given the results obtained for the A, B, C and D samples a second set of n$^+$/p homojunctions (samples W, X and Y) were produced with higher C_s and x_j values, as shown in Table 2.

Sample	C_s (at/cm^3)	x_j (μm)
W	5×10^{19}	3.0
X	5×10^{19}	2.5
Y	1×10^{20}	2.0

Tabela 2: The C_s and x_j parameters of the W, X and Y samples.

The sheet resistance of the unprocessed p-doped c-Si wafer R_S = 430 Ω/sq was measured with the FPP technique and the resistivity ρ = 12 Ω·cm was computed. The background B-concentration N_{bc}= 1×10^{16} at/cm^3 was obtained from a resistivity vs impurity concentration (p-Si) plot [22].

The Cs and x_j were computed from a concentration profile simulated in MATLAB. The simulation model fits both the concentration profiles obtained from eq. 8 and the profiles measured by SIMS in previous work done at the LMSCE [5].

The simulated Cs and x_j values alongside with the correspondent computed dopant dose after diffusion S are presented in Table. 3. The predeposited a-Si:H film thickness $d_{a-Si:H}$, the PH_3 gas phase concentration during deposition $[PH_3]$ and the diffusion time Δt_{diff} are presented in Table. 4.

Sample	C_s (at/cm^3)	x_j (μm)	S (at/cm^2)
A	5.1×10^{19}	0.99	2.4×10^{15}
B	5.7×10^{18}	0.97	4.6×10^{14}
C	5.5×10^{19}	1.99	4.9×10^{15}
D	5.5×10^{18}	1.99	6.4×10^{14}
W	5.7×10^{19}	3.04	8.8×10^{15}
X	5.7×10^{19}	2.47	8.0×10^{15}
Y	1.1×10^{20}	1.98	1.2×10^{16}

Tabela 3: The C_s, x_j and Ssimulated parameters of the A, B, C, D, W, X and Y samples.

The a-Si:H is deposited by PECVD, the PH_3 gas

Sample	$d_{a-Si:H}$ (nm)	$[PH_3]$ (%)	Δt_{diff} (min)
A	50	0.832	60
B	20	0.317	90
C	70	1.300	240
D	40	0.188	450
W	110	1.500	530
X	100	1.500	350
Y	100	2.300	410

Tabela 4: The $d_{a-Si:H}$, $[PH_3]$ and Δt_{diff} simulated parameters of the A, B, C, D, W, X and Y samples.

Sample	Δt_{diff} (min)	Δt_{ox} (min)	d_{ox} (nm)
A	60	15	215±4
B	90	6	153±6
C	240	20	284±7
D	450	13	270±7
W	530	42	278±7
X	350	37	(44±1) × 10
Y	210	37	(33±1) × 10

Tabela 7: The Δt_{diff}, Δt_{ox}, and d_{ox} (μm) parameters of the A, B, C, D, W, X and Y samples.

phase concentration $[PH_3]$, the SiH_4 flux F_{SiH_4} and the PH_3 flux F_{PH_3} are presented in Table 5. The total flux F_{Total} used during this process alongside with deposition time Δt_{dep} and the deposited a-Si.H film thickness $d_{a-Si:H}$ are presented in Table 6. After the a-Si:H deposition the lift-off technique was applied to each sample.

Sample	$[PH_3]$ (%)	F_{SiH_4} (SCCM)	F_{PH_3} (SCCM)
A	0.829	6.7	3.32
B	0.308	8.8	1.24
C	1.300	4.8	5.20
D	0.191	9.3	0.77
W	1.501	4.0	6.01
X	1.501	4.0	6.01
Y	2.255	1.0	9.21

Tabela 5: The $[PH_3]$, F_{SiH_4} and F_{PH_3} parameters of the A, B, C, D, W, X and Y samples.

Sample	F_{Total} (SCCM)	Δt_{dep} (mm:ss)	$d_{a-Si:H}$ (nm)
A	10.02	4:30	48 ± 2
B	10.04	2:15	23 ± 1
C	10.00	6:06	62 ±2
D	10.07	4:11	45 ±2
W	10.01	10:05	124 ±6
X	10.01	9:10	103 ±4
Y	10.21	9:00	113 ±6

Tabela 6: The F_{Total}, Δt_{dep} and $d_{a-Si:H}$ parameters of the A, B, C, D, W, X and Y samples.

Each sample was submitted to the a-Si:H dehydrogenation before diffusion. The thermal oxidation performed during the diffusion always occurred at the end of the process in order to minimize its influence on the diffusion. The diffusion time Δt_{diff}, the oxidation time Δt_{ox} and the SiO_2 thickness d_{ox} of each sample are presented in table. 7.

In order to measure the I-V characteristic, both front and back Al contacts (≈ 100 nm) were deposited on each sample followed by annealing.

3.2. Metal Contacts Application

The low performance of the solar cells described in the previous chapter could be related to the inability of conducting the generated current to the external circuit due to the low thickness of its metal contacts (≈100 nm). A c-Si commercial solar cell has a typical efficiency $\eta_{COM} \approx 17\%$ with a fill factor $FF_{COM} \approx 70\%$. Considering that these cells have a surface area $A_{COM} = 225$ cm^2, and the solar radiance at sea level $G \approx 100$ mW/cm^2, it comes for generated electric power $P_{COM} = G \times \eta_{COM} \times A_{COM} = 3.83$ W. Considering an open-circuit voltage $V_{OC_{COM}} = 0.7$ V, which is the usual value for commercial cells, and the P_{COM} computed, it comes for the short-circuited current $I_{SC_{COM}} = 7.81$ A. Performing the exact same computation for sample W presented in the previous chapter (with $A_W = 0.5$ cm^2, $V_{OC_W} = 0.49$ V, $FF_W = 64\%$, $\eta_W = 4.8\%$ and $G = 100$ mW/cm^2), it comes for the electric power generated and the short-circuited current, $P_W = 2.4$ mW and $I_{SC_W} = 7.6 \times 10^{-3}$ A, respectively. Considering for the metal contacts of these commercial solar cells a thickness $d_{COM} = 200$ μm, a width $w_{COM} = 2$mm and the electrical current computed previously, it comes for the density of electrical current $J_{COM} = 19.53 \times 10^2$ A/cm^2. Since sample W have metal contacts with width $w_W = 1$ mm, it must have a thickness $d_W = \frac{I_{SC_W}}{d_{COM} \times w_W} > 0.39$ μm in order to minimize current losses.

This thickness limitation comes from the small crucible size of the PVD system which is used for the Al deposition. In order to increase the thickness of the deposited Al using PVD, multiple depositions should be done which would be incovenient. Therefore, the electrodeposition of Cu which only requires an inexpensive simple set-up could be operative in this case. Since it is the first time that the Cu electrodeposition is done in the LMSCE an optimization of the process must be done in order to

find the adequate value of the current I that should be applied and the respective electrodeposition time Δt_{ED}.

A dry run was executed on a 2 cm^2 glass sample with a previously deposited Al layer ($d_{Al} \approx 100$ nm). A difficulty in the deposition of Cu on top of Al was observed. A second attempt was performed with a Cu seed layer ($d_{Cu} \approx 100$ nm) previously deposited on the Al layer by PVD. A smooth and uniform Cu growth on top of the seed layer was observed.

In order to find the optimal values for both the applied current I and the electrodeposition time Δt_{ED}, two studies were held. An area equal to the Al deposited metal contacts was delimeted in the sample by photolithography.

Firstly, the Δt_{ED} was held constant $\Delta t = 3$ min and the thickness of the deposited Cu was measured for five different values of I: I = 2 mA, I = 4 mA, I = 6 mA, I = 8 mA and I = 10 mA. The results are shown in Fig. 5

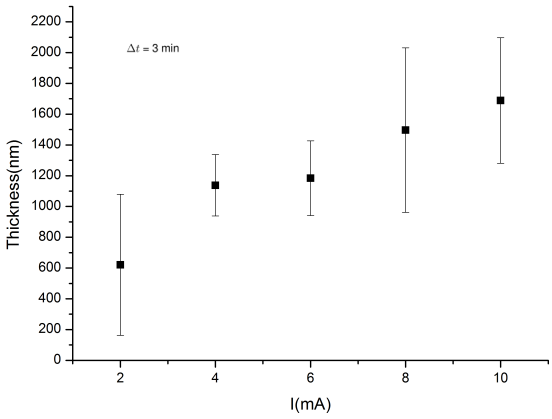

Figura 5: Electrodeposition study with constant Δt_{ED}: thickness as function of current for I = 2 mA, I = 4 mA, I = 6 mA, I = 8 mA and I = 10 mA.

Secondly, the I was held constant $I = 2$ mA and the thickness of the deposited Cu was measured for five different values of Δt_{ED}: $\Delta t_{ED} = 1$ min, $\Delta t_{ED} = 2$ min, $\Delta t_{ED} = 3$ min, $\Delta t_{ED} = 4$ min and $\Delta t_{ED} = 5$ min. The results are shown in Fig. 6.

Although the deposited Cu thickness increases with both the applied current (see Fig. 5) and the electrodeposition time (see Fig. 6) as expected, it was not possible to optimize the process since the results present an high disparity. This discrepancy in the measurements could be related to the difficulty of controlling the Cu electrode's area which is exposed to the $CuSO_4$. This adversity comes from the fact that during deposition the negatively charged sulfate ions would cover the Cu electrode reducing its exposed area to the solution. Moreover, since the Cu electrode is connected to the power supply by a crocodile clip which is not held fixed, the Cu electrode's area connected to the crocodile clip would fluctuate between measurements. Despite the inability of optimizing this process, it was decided to perform the Cu electrodeposition with the following parameters: $I = 2$ mA and $\Delta t_{ED} = 3$ min.

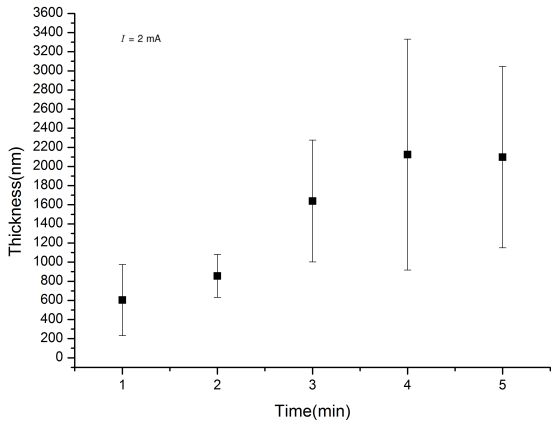

Figura 6: Electrodeposition study with constant I: thickness as function of Δt_{ED} for $\Delta t_{ED} = 1$ min, $\Delta t_{ED} = 2$ min, $\Delta t_{ED} = 3$ min, $\Delta t_{ED} = 4$ min and $\Delta t_{ED} = 5$ min.

This procedure was applied to sample W, described in the previous section, adding up a Cu layer with thickness $d_{Cu} \approx 2500nm$ to the previously deposited Al which resulted in a metal contact with total tickness $d_{Contact} \approx 2700$ nm.

4. Results

4.1. P-Diffusion Analysis

The sheet resistance R_{Sheet} of samples A, B, C and D were measured with the FPP technique and are presented in Table 8.

Sample	R_{Sheet} (Ω/sq)
A	95
B	314
C	78
D	250

Tabela 8: The R_{Sheet} of the A, B, C and D samples.

Samples A and C show considerable less R_{Sheet} than samples B and D. These results were expected since samples A and C have higher superficial dopant concentration ($C_s = 5{\times}10^{19}$ at/cm^3) than samples B and D ($C_s = 5{\times}10^{18}$ at/cm^3). The ob-

tained values are higher than the ones reached in previous work [8] [7]. This could be related to the existence of non-doped regions due to bad processing. These non-doped regions cause the recombination of carriers and consequently current losses.

The I-V characteristic curves of samples A, B, C and D in the dark are presented in Fig. 7.

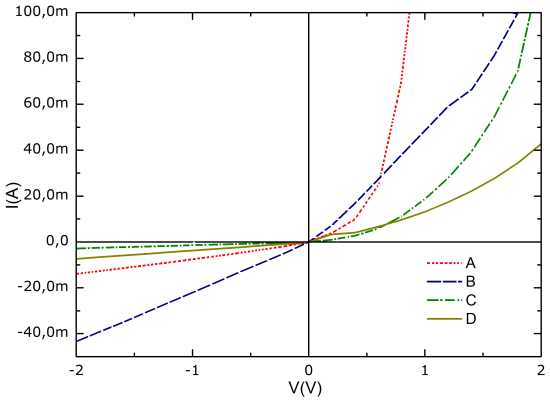

Figura 7: I-V characteristic curves A, B, C and D in the dark.

Samples A and B ($x_j = 1$ μm) do evidence significantly less rectifying ability in comparisson to samples C and D ($x_j = 2$ μm).

The high leakage current obtained in samples A and B could be originated by superficial defects in the Si/SiO_2 interface, the so-called network mismatch. These superficial defects could be reduced with hydrogen annealing in order to satisfy the dangling bonds. An impact study of the junction depth on the leakage current is found in the literature for Phosphorus doped Germanium (Ge) n^+/p homojunctions [9].

Given the results obtained from samples A, B, C and D, a new second set of n^+/p homojunctions (samples W, X and Y) were produced with higher superficial concentrations C_s and deeper junctions x_j.

The I-V characteristic semi-log curves of samples W, X and Y in the dark are presented in Fig. 8.

The I-V characteristic curves of samples W, X and Y under illumination are presented in Fig. 9.

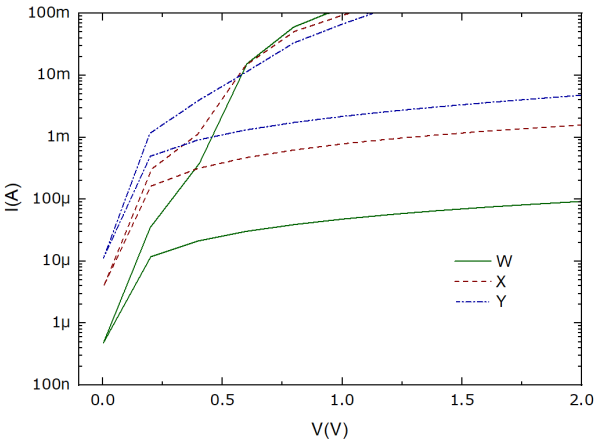

Figura 8: I-V characteristic semi-log curves W, X and Y in the dark.

As shown in Fig. 8, sample W ($x_j = 3$ μm) evidences a considerable higher rectifying ability than samples X ($x_j = 2.5$ μm) and Y ($x_j = 2$ μm). This result reinforces the idea that deeper junctions lead to less leakage current and consequently to an higher rectifying ability. Moreover, these results suggest that the P-doped c-Si Solar cells fabricated by the novel production method with superficial concentration ($5\times10^{18} < C_s < 5\times10^{19}$ at/cm^3) have an optimal junction depth higher than 2 μm, contrarily to similar solar cells fabricated by the conventional method as suggested in the literature [18]. The rectifying ability of sample W results in a higher maximum power point (MPP), as demonstrated in Fig. 9, and consequently in a higher fill factor.

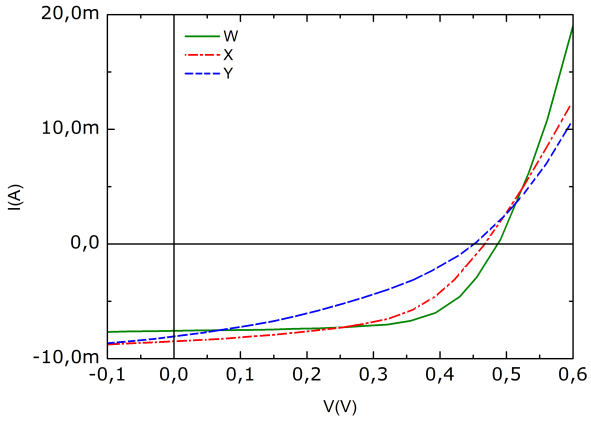

Figura 9: I-V characteristic curves W, X and Y under Illumination (artificial light that simulates a *quasi* AM1.5 spectrum).

The sheet resistance R_{Sheet}, the open-circuit voltage V_{OC}, the short-circuit current I_{SC} and the fill factor FF of samples W, X and Y are presented in Table 9. These values are compatible with the ones obtained in previous work [8] [7]. The improvement of these results in comparison to the ones obtained for samples A, B, C and D, could be related to the fact that samples W, X and Y have deeper junctions ($x_j > 2\mu$m).

Sample	R_{Sheet} (Ω/sq)	V_{OC} (V)	I_{SC} (mA)	FF
W	33	0.49	7.6	0.64
X	31	0.47	8.5	0.54
Y	25	0.45	8.1	0.36

Tabela 9: The R_{Sheet}, V_{OC}, I_{SC}, and FF parameters of the W, X and Y samples.

4.2. Metal Contacts Application

The I-V characteristic semi-log curves of sample W in the dark before and after the Cu electrodeposition are presented in Fig. 10 for comparison purposes.

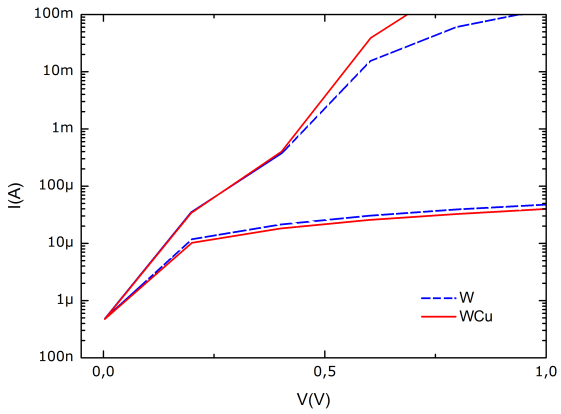

Figura 10: I-V characteristic semi-log curves of sample W in the dark before and after the Cu electrodeposition.

The I-V characteristic curves of sample W under illumination before and after the Cu electrodeposition are presented in Fig. 11.

The I-V characteristic semi-log curve of sample W in the dark after the Cu electrodeposition (red curve in Fig. 10), presents a current increase in the direct voltage biasing, high-current region relatively to the same sample before the Cu electrodeposition (blue curve in Fig. 10).

The I-V characteristic curve of sample under illumination after the Cu electrodeposition (red curve in Fig. 11), presents higher MPP than the same sample before the Cu electrodeposition (blue curve in Fig. 11).

The open-circuit voltage V_{OC}, the short-circuit current I_{SC} and the field factor FF of sample W before and after the Cu electrodeposition are presented in Table 10, the series resistanceR_S, the shunt resistance R_{Sh} an the efficiency η of sample W before and after the Cu electrodeposition are presented in Table 11.

Sample	V_{OC} (V)	I_{SC} (mA)	FF
W	0.49	7.6	0.64
WCu	0.48	7.7	0.70

Tabela 10: The V_{OC}, I_{SC} and FF parameters of sample W before and after the Cu electrodeposition.

Sample	R_S (Ω)	R_{Sh} (Ω)	η (%)
W	9.84	1.41×10^3	4.8
WCu	7.17	1.41×10^3	5.2

Tabela 11: The R_S, R_{Sh} and η parameters of sample W before and after the Cu electrodeposition.

The decrease of the series resistance R_S which resulted from the increase of the I(V) curve gradient near V_{OC} and consequently a horizontal displacement to the right of the MPP (Fig. 11), allied with the marginal increase of the I_{SC} (Table 10) led to an higher FF. This result is consistent with the hypothesis that previously applied Al contacts were not thick enough and were responsible for vol-

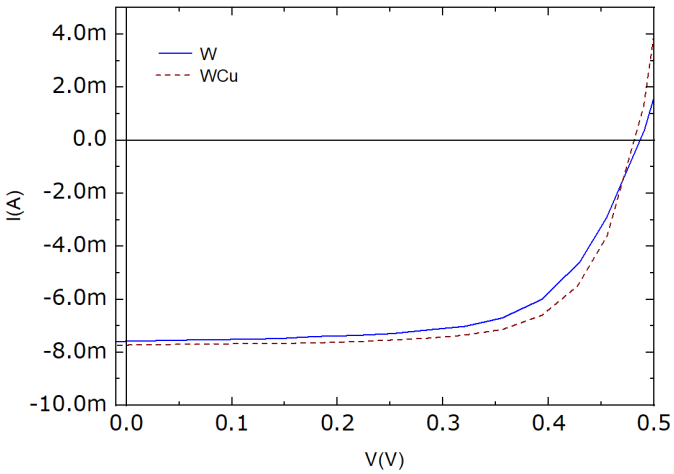

Figura 11: I-V characteristic curve of sample W under illumination (artificial light that simulates a *quasi* AM1.5 spectrum) before and after the Cu electrodeposition.

tage losses. On the other hand, the open-circuit voltage V_{OC} also presented a slightly lower value (less 10 mV), but it may be due to the measuring error.

The QE of sample W after the Cu electrodeposition was measured and is presented in Fig. 12 against a Si photodiode which was plotted as a reference.

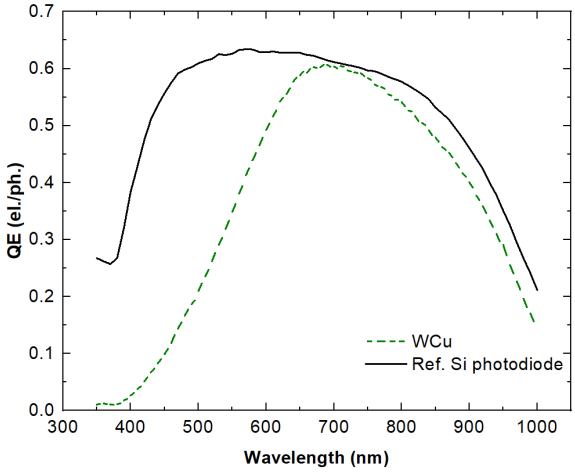

Figura 12: Quantum efficiency of sample W against a reference Si photodiode.

The quantum efficiency curve of sample W evidences a low absorption of radiation with wavelength $\lambda < 600$ nm in comparison to the Si photodiode. This low absorption of blue and green light could be due to the deep junction $x_j = 3$ μm of sample W, since this radiation is absorbed close to the surface and the carriers recombine before they reach the junction.

Despite the results presented in the previous section which supported that deeper junctions lead to an higher rectifying ability and consequently to a better performance of the solar cells, this result favours the use of shallower junctions in order to increase the absorption of blue and green light. Moreover, this hypothesis is consistent with the optimal junction depth value range ($1.2 < x_j < 2$ μm) for n-type highly P-doped c-Si solar cells determined by *Steam et al* [18]. In our case, the better rectifying ability showed by deeper junctions may be related with possible chemical impurities adsorbed near the surface, namely oxygen, which may be already present in a-Si:H. These impurities, even in low concentrations, when present in the space-charge region may disturb the junction electric field and degrade the rectifying ability. This is then solved by pushing the junction deep in the wafer, but with a worst Q.E in the blue

5. Conclusions

In this work a novel method for producing c-Si pn homojunctions, which replaces two steps at high temperatures from the conventional method, was improved for photovoltaic applications. Solar cells have been produced with an efficiency $\eta = 5.2\%$.

Interesting results were achieved with a study that focused on the superficial dopant concentration and the homojunction depth. P-doped c-Si Solar cells fabricated by this novel production method, with superficial concentration ($5\times10^{18} < C_s < 5\times10^{19}$ at/cm^3), have an optimal junction depth higher than 2 μm, contrarily to similar solar cells fabricated by the conventional method as suggested in the literature [18]. This may be related with possible chemical impurities adsorbed near the surface, namely oxygen, which may be already present in a-Si:H. These impurities, even in low concentrations, when present in the space-charge region may disturb the junction electric field and degrade the rectifying ability.

Positive results were obtained from a study which improved the performance of these solar cells by thickening their metal contacts. A decrease of the series resistance R_S was observed,which resulted from the increase of the I(V) curve gradient near the open-circuit voltage V_{OC} and consequently a horizontal displacement to the right of the MPP, allied with the marginal increase of the short-circuit current I_{SC} which led to an higher field factor FF.

A QE measurement of the best performing sample demonstrated a low absorption of radiation with wavelength $\lambda < 600$ nm in comparison to a reference Si photodiode. This low absorption of blue and green light could be due to the deep junction $x_j = 3$ μm of the sample, since this radiation is absorbed close to the surface and the carriers recombine before they reach the junction.

This work has proven that this novel production method is perfectly capable of producing c-Si pn homojunctions for photovoltaic applications. A 0.4% improvements were accomplished by optimizing the superficial concentration and thickening the metals contacts. As future work, interesting results should be expected by reducing the chemical impurities near the surface and decreasing the junction depth in order to increase the absorption of blue wavelength light.

Acknowledgements

Firstly, I would like to thank my supervisors, Prof. Guilherme Lavareda and Prof. Ana de Amaral, for their help and guidance during the making of this thesis. I am particularly grateful to Prof. Guilherme Lavareda for his tremendous support and patience, and with whom I've learnt a lot about physics and materials science. Secondly, I would

like to thank Yuri Vygranenko for his contribution with the spectral response measurement. I would also like to thank Prof. Carlos Nunes de Carvalho for his useful advice. Finally, I would like to thank my family and friends for their invaluable support.

Referências

[1] A. Bentzen and A. Holt. Overview of phosphorus diffusion and gettering in multicrystalline silicon. *Materials Science and Engineering: B*, 159:228–234, 2009. DOI: 10.1016/j.mseb.2008.10.060.

[2] T. M. Bruton. General trends about photovoltaics based on crystalline silicon. *Solar Energy Materials & Solar Cells*, (72):3–7, 2002. DOI: 10.1016/S0927-0248(01)00145-3.

[3] J. A. Carson. *Solar Cell Research Progress*. Nova Science Publishers, Inc., 2008.

[4] D. M. Chapin, C. S. Fuller, and G. L. Pearson. A new p–n junction photocell for converting solar radiation into electrical power. *J Appl Phys*, (25):676–7, 1954. DOI: 10.1063/1.1721711.

[5] A. de Calheiros Velozo. Crystalline silicon photovoltaic solar cells using amorphous silicon as dopant source. Master's thesis, University of Lisbon, 2012.

[6] A. de Calheiros Velozo, G. Lavareda, C. N. de Carvalho, and A. Amaral. Thermal dehydrogenation of amorphous silicon deposited on c-si: Effect of the substrate temperature during deposition. *Phys. Status Solidi C*, 9(10-11):2198–2202, 2012. DOI: 10.1002/pssc.201200194.

[7] D. T. M. de Jesus Vicente. Células fotovoltaicas de silício cristalino: homojunções obtidas pelo método de prédeposição de dopante a baixa temperatura e heterojunções hit, school = Universidade Nova de Lisboa, year = 2014, optional fields: type = , address = , month = , note = . Master's thesis.

[8] L. S. do Carmo Ricardo. Transístores de efeito de campo de silício cristalino obtidos pelo método de pré-deposição de dopante a baixa temperatura. Master's thesis, Universidade Nova de Lisboa, 2014.

[9] W. Hsu, A. Rai, X. Wang, Y. Wang, T. Kim, and S. K. Banerje. Impact of junction depth and abruptness on the activation and the leakage current in germanium n+/p junctions. *arXiv:1705.06733*, 2017.

[10] C. Hu. *Modern Semiconductor Devices for Integrated Circuits*. Pearson, 2010.

[11] J. P. Joly. Metallic contamination of silicon wafers. *Microelectronic Engineering*, (40):285, 1998. DOI: 10.1016/S0167-9317(98)00278-0.

[12] S. W. Jones. Diffusion in silicon, 2000.

[13] G. Lavareda, A. C. Velozo, C. de Carvalho, and A.Amaral. p/n junction depth control using amorphous silicon as a low temperature dopant source. *Thin Solid Films*, 543:122–124, 2013. DOI: 10.1016/j.tsf.2013.02.043.

[14] T. Markvart. *Solar Electricity*. Wiley, 2000.

[15] A. Polman, M. Knight, E. C. Garnet, B. Ehrler, and W. C. Sinke. Photovoltaic materials: Present efficiencies and future challenges. *Science*, 352(6283), 2016. DOI: 10.1126/science.aad4424.

[16] W. S. Ruska. *Microelectronic processing : An introduction to the manufacture of integrated circuits*. McGraw-Hill, 1988.

[17] A. Sayigh. *Comprehensive Renewable Energy*. Elsevier, 2012.

[18] N. Stem and M. Cid. Studies of phosphorus gaussian profile emitter silicon solar cells. *Materials Research*, 4(2):143–148, 2001. DOI: 10.1016/0379-6787(91)90092-4.

[19] B. G. Streetman. *Solid state electronic devices*. Prentice Hall, 2000.

[20] S. M. Sze. *Semiconductor Devices Physics and Technology*. Wiley, 2002.

[21] M. Thirugnanasambandam, S. Iniyan, and R. Goicc. A review of solar thermal technologies. *Renewable and Sustainable Energy Reviews*, (14):312–22, 2010. DOI: 10.1016/j.rser.2009.07.014.

[22] W. R. Thurber, R. L. Mattis, and Y. M. Liu. *Semiconductor Measurement Technology: The Relationship Between Resistivity and Dopant Density for Phosphorusand Boron-Doped Silicon*. National Bureau of Standards Special Publication 400-64l, 1981.

[23] J. K. Casper. *Fossil Fuels and Pollution: The Future of Air Quality*. Infobase Publishing, 2010.

[24] A. Demirbas. *Biodiesel: A Realistic Fuel Alternative for Diesel Engines*. Springer, 2007.

[25] A. Demirbas. *Biofuels: Securing the Planet's Future Energy Needs*. Springer, 2008.

[26] Y. T. Shah. *Thermal Energy: Sources, Recovery, and Applications*. CRC Press, 2018.